

Article

Effects of Ground Heating on Ventilation and Pollutant Transport in Three-Dimensional Urban Street Canyons with Unit Aspect Ratio

Guoyi Jiang ^{1,*} , Tingting Hu ² and Haokai Yang ¹

¹ Department of civil and environmental engineering, Shantou University, Shantou 515063, China; 15hkyang@stu.edu.cn

² College of Chemistry and Chemical Engineering, Shanghai University of Engineering Science, Shanghai 201620, China; tingtinghu@sues.edu.cn

* Correspondence: gyjiang@stu.edu.cn; Tel.: +86-0754-8650-3261

Received: 23 April 2019; Accepted: 17 May 2019; Published: 21 May 2019



Abstract: A validated standard k - ε model was used to investigate the effects of ground heating on ventilation and pollutant transport in a three-dimensional (3D) street canyon. Air entered the street canyon from the upper regions of side surfaces and most areas of the top surface and left from the lower regions of side surfaces. Ground heating enhanced the mean flow, ventilation, and turbulence, and facilitated pollutant reduction inside street canyons. The transport patterns in a street canyon that included a pollutant source (PSC) and a target street canyon downstream (TSC) were different. The pollutant did not enter the PSC, and turbulent diffusion dominated pollutant outflow at all boundaries. The pollutant entered the TSC from most regions of the side surfaces and exited from lower regions of the side surfaces and the entire top surface. Air convection dominated pollutant transport at the side surfaces, and its contribution increased significantly with ground temperature; Furthermore, turbulent diffusion dominated pollutant outflow for the top surface, and its contribution increased slightly with ground heating. As revealed by an analysis of both the total pollutant flow rates and air flow rates, although air/pollutant exchange between the TSC and outer space occurred primarily through the side surfaces, the increase in air inflow from the top surface reduced the pollutant concentration inside the street canyon when the ground temperature increased. The top surface played a major role in improving air quality in a 3D environment with ground dispersion. This study supplied valuable suggestions for urban planning strategies. The analyzing method used in this research is helpful for the pollutant transport investigations in urban areas.

Keywords: street canyon; ground heating; ventilation; pollutant transport; computational fluid dynamics (CFD); Reynolds-Averaged Navier-Stokes (RANS)

1. Introduction

Urban street canyons are located at the bottom of a turbulent atmospheric boundary layer. They typically exhibit a distinct climate in which usually the microscale meteorological processes dominate [1]. With the increase in urbanization and human activities, the deterioration of air quality in urban environment has caused serious problems for people living inside street canyons. Better ventilating performance is considered an effective countermeasure to improve the thermal environment and air quality inside street canyons.

The most critical factors influencing ventilation and pollutant transport/dispersion in urban areas are the aspect ratio of the street canyon (building-height-to-street-width) and ground/building facade heating due to absorption of solar radiation in summer. A two-dimensional (2D) idealized

street canyon, which is a generic unit of a city, constitutes the platform for gaining a fundamental understanding of ventilation and pollutant removal at the neighborhood scale [2]. Computational fluid dynamics (CFD) has been used to study the effects of aspect ratio on air flow, pollutant dispersion, and their exchange phenomena in a 2D urban street canyon [2–4]. In urban areas, the ground temperature usually changes considerably at different times of day, or in different seasons, thereby affecting air flow and pollutant dispersion. Li et al. [5] and Cheng and Liu [6] have used large-eddy simulation (LES) to investigate the effect of thermal stability on air flow and dispersion characteristics inside a 2D street canyon with unit aspect ratio. Different thermal stratifications were produced by heating or cooling the ground to different temperatures. The results showed that ground heating considerably enhanced the mean flow, turbulence, and pollutant flux inside the street canyon. Mildly improved pollutant removal under stronger ground heating conditions was observed because of the enhanced roof-level buoyancy-driven turbulence. Xie et al. [7] used Reynolds-Averaged Navier-Stokes (RANS) equations to investigate the impact of ground heating on air flow and air exchange in an idealized 2D street canyon with unit aspect ratio. The CFD results revealed that the existence of a buoyancy force markedly affected the airflow structure and air exchange rate and that the air exchange rate induced by vertical velocity fluctuation was larger than that induced by mean vertical velocity.

Cheng et al. [8] used a RANS model to examine ventilation and pollutant transport in a 2D street canyon with unit aspect ratio under different unstable stratifications generated by heating all solid boundaries (streets, building facades, and roofs). The results suggested that unstable stratification promotes ventilation in street canyons. Turbulent transport dominates pollutant removal under isothermal conditions; however, progressive dominance by mean wind can be observed with increasing thermal stratification. Allegrini et al. [9] conducted wind tunnel measurements to study the effect of buoyancy on air flow in a scaled 2D street canyon. The two walls and bottom surface of the street canyon were heated either separately or simultaneously. The results showed that the main vortex and turbulent kinetic energy inside the street canyon were strengthened by the heating of the ground, leeward wall, and all three surfaces for low free-stream velocities. However, the flow structures were different for windward wall heating. Kim and Baik [10] used a 2D RANS model to investigate street-canyon flows with various aspect ratios and street-bottom heating cases. Li et al. [11] employed a validated LES model to study the combined effects of aspect ratio and ground heating on 2D urban-canyon flow and dispersion. Considerable changes in flow and scalar patterns were caused by ground heating for street canyons with aspect ratios of 2 and 0.5. Xie et al. [12] adopted the RANS model to investigate the effects of aspect ratio, building facades, and ground heating on wind flow and pollutant transport in 2D street canyons; they found complicated wind flow and pollutant transport due to the existence of buoyancy. With the increasing use of CFD techniques, it is crucial to assess the performance of turbulence models adopted to estimate ventilation and pollutant dispersion in urban areas. Evaluations of turbulence models and physical parameters influencing CFD simulations have been conducted by Chatzimichailidis et al. [13] for 2D street-canyon flows, by Tominaga and Stathopoulos [14] for three-dimensional (3D) street-canyon flows, by Dai et al. [15] through flow and dispersion inside building arrays, and by Yoshie et al. [16] through a simulation of flow and dispersion around a high-rise building under a weakly unstable condition. Chew et al. [17] evaluated the performance of RANS and LES models in the simulations of reduced-scale and full-scale 2D street-canyon flows with windward wall heating. The LES results were highly consistent with measurements at both scales. RANS models perform well at reduced scale but over-predict the thermal effects of heated windward walls at full scale.

The aforementioned studies have focused on only buoyant flow and dispersion inside 2D street canyons. However, ventilation and pollutant transport can occur through both of the side boundaries and the top surface of a 3D street canyon. Therefore studies on the effects of buoyancy on 3D street-canyon flow have attracted attention. Uehara et al. [18] investigated the effects of atmospheric stability on flow in 3D street canyons with simple-shaped blocks by using a thermally stratified wind tunnel. They found that cavity eddies were weak when the atmosphere was stable and strong under

unstable conditions. However, they considered only the flow in a vertical plane and not 3D flow structures. Kim and Baik [19] used an unsteady RANS model to study the effects of street-bottom and building-roof heating on flow in a 3D street canyon with unit aspect ratio. Their results showed that the mean kinetic energy and vorticity inside the street canyon increased for purely street-bottom heating but weakened in the presence of both street-bottom and building-roof heating. Allegrini [20] conducted wind tunnel experiments to investigate the effects of building length and roof shape on 3D buoyant flow inside street canyons. They measured flow structures by using particle image velocimetry in both horizontal and vertical planes. Nazarian and Kleissl [21] performed numerical simulations to analyze the effect of non-uniform thermal forcing on mean flow, turbulence statistics, temperature, and canyon ventilation. Jiang and Yoshie [22] simulated the flow and pollutant dispersion in a 3D thermal environment at reduced scale, evaluated the performance of an LES model, and studied turbulence statistics and pollutant transport mechanisms in a 3D street canyon.

The unstable stratifications are quite common atmospheric phenomena because of the absorption of the solar radiations by the ground in summer or the human activities in urban areas. As a result, the air flow and ventilation are strongly affected by the buoyancy effect due to the existence of the temperature difference. The affected ventilation performance is closely related to the thermal environment and air quality inside a street canyon where people are living. In most realistic urban environments, both the air flow and pollutant dispersion are 3D. Therefore, studies on ventilation and dispersion in a 3D thermal environment are important for understanding the basic pollutant transport phenomena, so that countermeasures can be taken to improve the air quality inside a street canyon. As mentioned, many studies have investigated the buoyancy effect on air flow, ventilation, and pollutant dispersion, but such investigations have primarily been conducted for 2D street canyons. For a 2D street canyon, the top boundary is the only place where ventilation and pollutant exchange can occur. Although several studies have investigated the effect of buoyancy on flow structures in a 3D street canyon, very few have addressed the ventilation and pollutant dispersion phenomena. So the basic pollutant transport phenomena affected by the ground heating are still not clear in a 3D environment. In this study, a validated RANS model based on a standard $k-\varepsilon$ closure was adopted to investigate the effects of ground heating on air flow, ventilation, and pollutant transport in a 3D urban environment with a cubical block arrangement. A line source was placed at the middle ground of the building group to characterize the pollutant source. Because pollutant transport patterns are quite different inside different street canyons along the streamwise direction, pollutant transport behaviors for both a street canyon that includes a pollutant source and a target street canyon downstream were investigated; however, this study focused on the target street canyon downstream because transport processes were more complicated inside this street canyon.

2. Method for Calculating Air and Pollutant Flow Rates

The boundary surfaces of a 3D street canyon are the direct areas in which ventilation and pollutant exchange between inner and outer spaces occur. Ventilation is characterized by the air flow rates at the boundaries, and pollutant exchange is characterized by the pollutant flow rates in this study. Figure 1 shows the three boundaries (one top surface, two side surfaces) of a 3D street canyon, which are marked by “Top”, “Left”, and “Right”. At each surface, the velocity component perpendicular to the boundary can be used to calculate the air flow rate. Total air inflow rates and air outflow rates at each boundary can be calculated as follows:

$$\Delta q_{a,in} = \sum_{i=1}^m \rho A_i \langle u_{ni} \rangle, \quad \Delta q_{a,out} = \sum_{j=1}^k \rho A_j \langle u_{nj} \rangle \quad (\text{kg/s}) \quad (1)$$

where $\langle \rangle$ is the ensemble average; ρ , the density of air; A_i , the area of the i th mesh face; u_n , the instantaneous velocity component perpendicular to the mesh face. The vertical velocity component w is used for the top surface, and the lateral velocity component v is used for the side surfaces. At the

top surface, a positive w value signifies air outflow. For the left surface, a positive v value signifies air outflow, and for the right surface, a negative v value signifies outflow. In Equation (1), $m + k$ should equal the total mesh faces at one boundary surface.

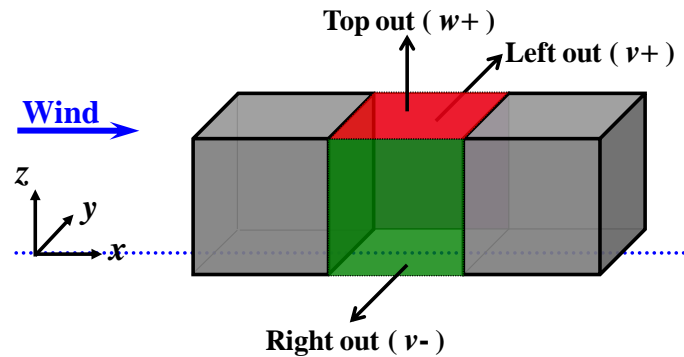


Figure 1. Sketch of three boundaries of a 3D street canyon and outflow definition.

In turbulence statistics, if an instantaneous variable is decomposed into its mean and fluctuating components, then the total pollutant flux (ensemble-averaged mean pollutant flux) can be calculated as follows:

$$\langle u_j c \rangle = \langle u_j \rangle \langle c \rangle + \langle u'_j c' \rangle \tag{2}$$

where, u_j is the instantaneous velocity component ($j = 1, 2, 3$) and c , the instantaneous pollutant concentration. In the LES model, all three terms can be obtained by performing time averaging in the simulation. In the RANS model, the first and second terms on the right-hand side of Equation (2) are usually referred to as convective flux and turbulent diffusion flux, respectively. Convective flux can be obtained immediately after the equations have been solved, and turbulent diffusion flux can be obtained according to the following gradient diffusion hypothesis (or eddy viscosity model) adopted in most RANS turbulence modeling approaches [23,24]:

$$\langle u'_j c' \rangle = -\frac{\nu_t}{Sc_t} \cdot \frac{\partial C}{\partial x_j} \tag{3}$$

where, ν_t is the turbulent viscosity; Sc_t , the turbulent Schmidt number; C , the mean pollutant concentration; and x_j ($j = 1, 2, 3$), the three components of space coordinates. At the boundaries of a street canyon, only the velocity component in the normal direction is responsible for pollutant removal or entering; therefore, the mass flow rate of pollutant in each mesh face can be calculated from the total pollutant flux as follows:

$$\rho A_i \langle u_{ni} c_i \rangle = \rho A_i \langle u_{ni} \rangle \langle c_i \rangle + \rho A_i \langle u'_{ni} c'_i \rangle \tag{4}$$

The sign of the pollutant flow rate indicates whether pollutants enter or leave the street canyon through this mesh face. For the top and left surfaces, a positive value represents pollutant outflow and a negative value represents pollutant inflow; the opposite is true for the right surface. If the same effects (enters or leaves) are added together at one boundary surface, then the total pollutant inflow or outflow rates at this boundary of the street canyon can be calculated as follows:

$$\Delta q_{p, in} = \sum_{i=1}^m \rho A_i \langle u_{ni} c_i \rangle, \Delta q_{p, out} = \sum_{j=1}^k \rho A_j \langle u_{nj} c_j \rangle \quad (\text{kg/s}) \tag{5}$$

Equation (4) shows that the pollutant flow rate in each mesh face includes contributions by both air convection and turbulent diffusion. In general, the signs of the two right-hand-side terms are not the same, indicating that they may have different contributions to pollutant transport into or out of the street canyon. Although pollutant flow rate can be obtained if the two right-hand-side terms of

Equation (4) are added algebraically, their individual contributions will disappear. When individual effects must be determined, then the two right-hand-side terms of Equation (4) can be considered separately for each mesh face. The pollutant inflow or outflow rates contributed by air convection or turbulent diffusion at one boundary of the street canyon can then be calculated from the convective flux or turbulent diffusion flux as follows:

$$\Delta q_{p, in} = \sum_{i=1}^{m_1} \rho A_i \langle u_{ni} \rangle \langle c_i \rangle, \quad \Delta q_{p, out} = \sum_{j=1}^{k_1} \rho A_j \langle u_{nj} \rangle \langle c_j \rangle \quad (\text{kg/s}) \quad (6)$$

$$\Delta q_{p, in} = \sum_{i=1}^{m_2} \rho A_i \langle u'_{ni} c'_i \rangle, \quad \Delta q_{p, out} = \sum_{j=1}^{k_2} \rho A_j \langle u'_{nj} c'_j \rangle \quad (\text{kg/s}) \quad (7)$$

where both $m_1 + k_1$ and $m_2 + k_2$ should equal the total mesh faces at one boundary surface.

3. Validations of Computational Fluid Dynamics (CFD) Model

This study performed steady simulations using the RANS model. The selection of the turbulence models is the first and crucial step to ensure the prediction accuracy of simulations. Xie et al. [25] compared the accuracy of standard, RNG, and Chen-Kim $k-\varepsilon$ models with wind tunnel measurements for 2D street-canyon flows and dispersion. They found that the standard $k-\varepsilon$ model (SKE) provided the most reliable results. The Architectural Institute of Japan (AIJ) has performed comparisons of various $k-\varepsilon$ models, DSM and LES applied to flow around a high-rise building and in urban areas [26–28]. Among all tested models, the LES model provided the best results. Although the revised $k-\varepsilon$ models could reproduce the reverse flow on the roof, they overestimated the reattachment length behind the building. Compared with the revised models, the velocity calculated by the SKE model showed the best agreement with the experiment in weak wind regions such as behind the buildings and within street canyons. The SKE model was selected in this study because the environmental issues are concerned. Further evaluation of the accuracy of the SKE model for flow and dispersion in a 3D thermal environment was performed through comparisons with wind tunnel experiments in this study.

The experiments reported by Jiang and Yoshie [22] were used to validate the current SKE model. An urban street model with cubical building blocks (size $h = 60$ mm) of 14 rows \times 9 columns was placed in an unstable boundary layer. The temperature of the wind tunnel floor was controlled uniformly at 45 °C. Both the mean inflow velocity and temperature profiles followed logarithmic laws; $U_h = 1.34$ m/s was the mean streamwise velocity at the building height position. A line source with 37-mm width was placed at the middle ground between the seventh and the eighth rows of the building blocks. Tracer gas ethylene (100% C_2H_4 , 35 °C) was released to the flow field at a volume flow rate of $q_0 = 8.33 \times 10^{-6}$ m³/s. The reference concentration was $C_0 = q_0 / (U_h h^2)$. The LES result reported in this study was also used to evaluate the current SKE model.

Figure 2 shows comparisons of the normalized mean streamwise velocity and mean concentration in a vertical centerline located between the eighth and ninth rows of the building blocks. As illustrated in Figure 2a, the difference between the mean streamwise velocities predicted by the SKE and LES models is quite small, and both CFD results are in good agreement with the experiment in this vertical centerline. Because the turbulent Schmidt number (Sc_t) is essential for predicting a concentration field when a RANS model is adopted, this value must be selected carefully. Tominaga and Stathopoulos [29] reviewed studies on the selection of Sc_t for engineering applications, and the optimum values are widely distributed in the range of 0.2–1.3. The influence of different Sc_t values on the predicted concentration field was also examined in this study. As shown in Figure 2b, large differences are observed for the predicted concentration field. Although the concentration is somewhat underestimated by the LES model, the distribution pattern predicted by the LES model is more similar to the experiment compared with that predicted by the SKE model. A higher Sc_t value lead to overestimation of the concentration field in the SKE model, and $Sc_t = 0.4$ provides the best result. Although not shown here, when the

comparisons are concerned in a horizontal direction at a ground level, the LES results showed the best agreement with the experiment. The mean streamwise velocity was a little underestimated and the mean concentration was overestimated by the SKE model in the passageways (or channels) between the columns.

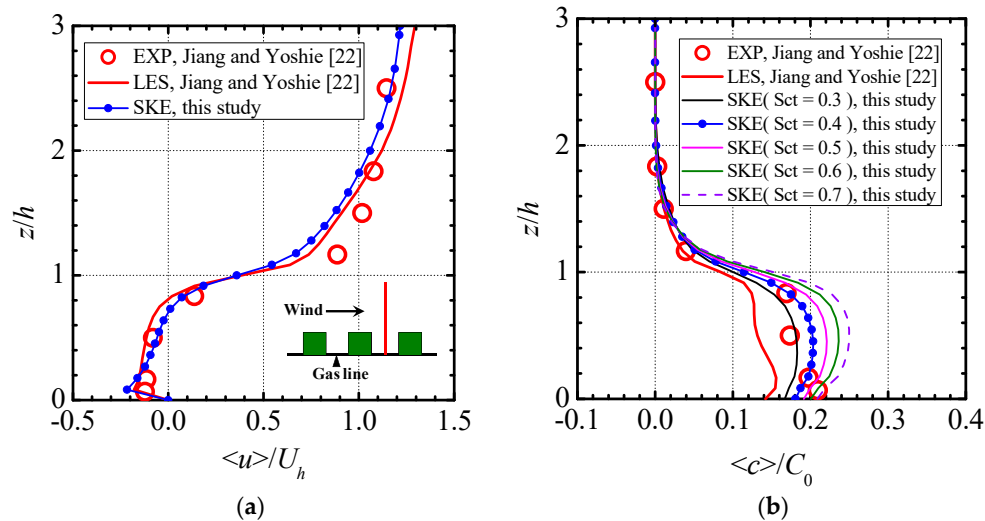


Figure 2. Vertical distributions of mean flow variables: (a) normalized mean streamwise velocity; (b) normalized mean concentration.

The performance of the SKE model in calculating air flow rates in a 3D street canyon was evaluated through comparisons with the LES results, as presented in Figure 3. This street canyon was located in the middle column between the blocks of the eighth and ninth rows. $q' = \rho U_h h^2$ was used to normalize the air flow rates. In Figure 3, the blue and pink charts indicate the air inflow and outflow rates, respectively. The LES results show that for both the side and top surfaces, the difference between the air inflow and outflow rates is nonsignificant. The air flow rates at the side surfaces are much higher than those at the top surface. The air flow rates calculated by the SKE model are quite similar to the LES results, although they are slightly underestimated at the top surface. Overall, the prediction accuracy of the SKE model is satisfactory if an appropriate Sc_t value is selected, and the SKE model can be used to investigate the ventilation and dispersion phenomena in a 3D thermal environment. Another benefit of using RANS model is that the full-scale simulations can be conducted.

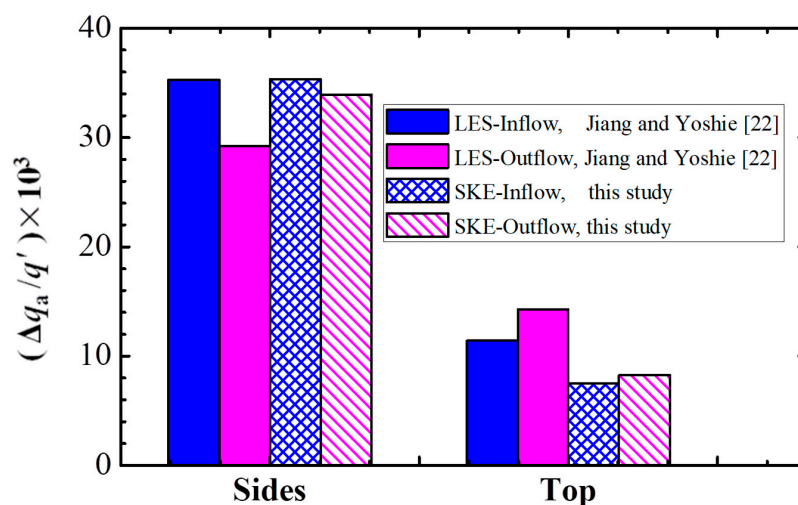


Figure 3. Comparison of air flow rates between standard $k-\epsilon$ model (SKE) and large-eddy simulation (LES).

4. Model Description and Setup

Figure 4 shows the computational domain and setup of the simulation. A building group with eight rows of cubical building blocks was placed within a surface boundary layer. The size of each cubical building block was $H = 10$ m, and the blocks were placed at equal distances of 10 m from each other on the ground. Thus, the aspect ratio of the street canyon was 1. A pollutant line source with a width of $W = 3$ m was placed at the middle ground between the fourth and fifth rows of the blocks. Because this study used a line source, both the flow and the dispersion would be symmetrical along the vertical center plane of any column if the number of columns was infinite in the spanwise direction. Therefore, the vertical center planes of the two columns beside the middle column were selected as the side boundaries, and a symmetry condition was used to indicate that the columns were infinitely repeated in the spanwise direction. Except for the number of building blocks, the simulation arrangement was similar to the reduced-scale experiment described in Section 3; however full-scale simulations were conducted in this study. Two street canyons were selected in this study to investigate flow and dispersion phenomena: (1) a street canyon containing a pollutant source and located in the middle column and between the blocks of the fourth and fifth rows (PSC), and (2) a target street canyon downstream (TSC). Because the pollutant discharge line still had a little influence on the flow field at the ground level, only the flow structures in the TSC are presented in this paper. The pollutant transport behaviors were investigated for both the PSC and TSC.

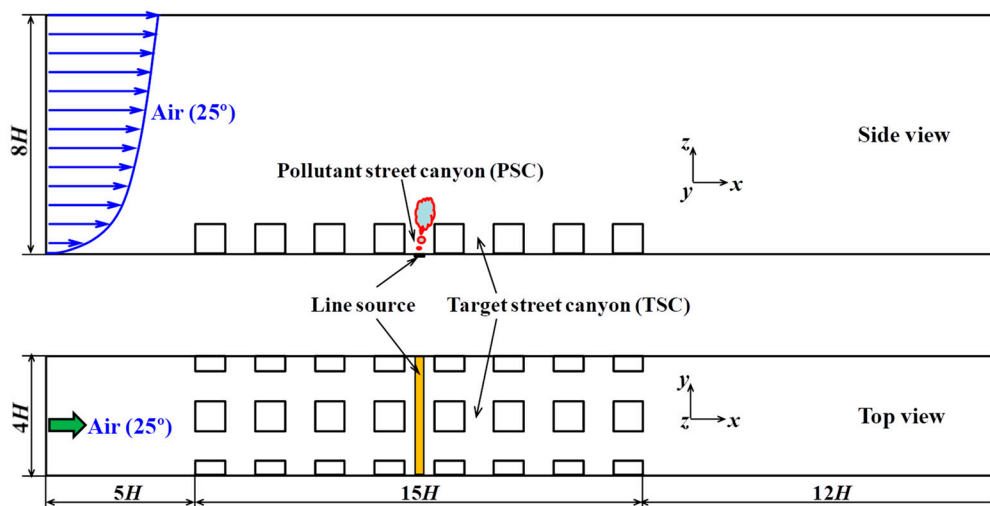


Figure 4. Computational domain and setup of the simulation.

The inflow mean wind velocity profile and turbulent profiles were selected according to AIJ recommendations in the wind engineering field [30], and they are expressed as follows:

$$U_z = U_H \left(\frac{z}{H} \right)^\alpha \tag{8}$$

$$k = (I_z \cdot U_z)^2 \tag{9}$$

$$I_z = 0.1 \times \left(\frac{z}{z_G} \right)^{(-\alpha-0.05)} \tag{10}$$

$$\varepsilon = C_\mu^{1/2} \cdot k \cdot \frac{dU_z}{dz} \tag{11}$$

where, H is the height of the building blocks. U_H is the mean wind velocity at height H , and a weak wind flow of $U_H = 3$ m/s was selected in this study. Moreover, α is the power-law exponent determined by terrain category; $\alpha = 0.15$ was set in this study to simulate B-type terrain roughness in both Chinese

and Japanese codes. k and ε are the turbulent kinetic energy and turbulent dissipation rate, respectively. I_z is the turbulence intensity profile, and z_G is the height of the boundary layer; $z_G = 350$ m for the B-type category.

The temperature of incoming air was set to $\Theta_a = 25$ °C for all cases to indicate a cool air inflow condition. Different unstable thermal stratifications were generated by different temperature settings at the ground. The bulk Richardson number Rb was used to indicate different thermal stability levels, and it is defined as follows:

$$Rb = -\frac{g\beta H \cdot (\Theta_a - \Theta_f)}{U_H^2} \quad (12)$$

where $g = -9.8$ m/s² is the gravitational acceleration; β , the thermal expansion rate; and Θ_f , the ground temperature. Table 1 summarizes the simulation cases. According to field measurements conducted by Niachou et al. [31] in Athens, Greece, during the summer of 2002, the maximum surface temperature of an asphalt street inside a street canyon can reach approximately 64 °C at midday due to the vertical incidence of solar radiation. In this study, the ground temperature was set from 25 °C to 65 °C, with a 5 °C difference from different cases. Nine simulation cases were tested in this study to investigate the effect of ground heating on ventilation and dispersion phenomena; these covered a range from neutral condition (GH-25, $Rb = 0$) to a strong unstable condition (GH-65, $Rb = -1.44$).

Table 1. Simulation cases.

Case Names	Ground Heating	Rb
1. GH-25	25 °C	0
2. GH-30	30 °C	-0.18
3. GH-35	35 °C	-0.36
4. GH-40	40 °C	-0.54
5. GH-45	45 °C	-0.72
6. GH-50	50 °C	-0.90
7. GH-55	55 °C	-1.08
8. GH-60	60 °C	-1.26
9. GH-65	65 °C	-1.44

Steady simulations using SKE model were performed in this study. The solved governing equations included continuity, momentum, energy, and transport equations for turbulent kinetic energy k and turbulent dissipation rate ε . The Boussinesq approximation was used for the buoyancy term in the momentum equation, and the gravitational acceleration was set to $g = -9.8$ m/s². The effect of buoyancy on the k and ε equations was considered to ensure that the full buoyancy effect was taken into account. The turbulent Prandtl number was set to 0.9. A passive scalar transport equation was solved to simulate pollutant dispersion in the air, and $Sc_t = 0.4$ was set, as confirmed in previous validations through a reduced-scale experiment. The QUICK scheme was used for discretizing the convection term in the momentum equation. The SIMPLE algorithm was used for the pressure-velocity calculation.

The boundary layer profiles (Equations (8)–(11)) recommended by AIJ were proposed as inflow conditions. The outlet boundary was located at a distance of $12H$ from the back surface of the last row of the building blocks, and a zero-gradient condition was used for the outlet boundary. The height of the domain was $8H$, and a symmetry condition was adopted for the top boundary. The width of the domain was $4H$, and symmetry conditions were used for the two side boundaries to indicate that both the geometry and the flow/dispersion were infinitely repeated in the spanwise direction. The width of the pollutant discharge line was $W = 3$ m in the streamwise direction, and a small mass flow rate of $q_p = 1.47 \times 10^{-3}$ kg/s (100%) was used to reduce the effect of gas discharging on the flow field. The reference concentration was $C^* = q_p / (\rho U_H H^2)$. The temperature of the discharged pollutant was set to 25 °C (same as that of incoming air). Notably, thermal stabilities are usually stronger for full-scale simulations, and setting a higher temperature for the discharged pollutant may destroy the normal

flow structures inside the street canyon. The wall boundary conditions were used for the ground and building surfaces. The temperature of building surfaces was set to 25 °C, and different ground temperatures were given to generate different heating intensities. For full-scale simulations, capturing near-wall flows is currently impossible owing to computational limitations; therefore, wall functions were used to model the near-wall flow, and this is the best choice when high-Reynolds-number RANS models are used in most engineering fields. Hexahedral mesh systems were used for the simulations. The influence of mesh density on the simulations was checked through the case of GH-30 using three mesh systems (1,000,000, 3,000,000 and 4,000,000 cell numbers). The results showed that slight differences existed between the first and the final two mesh systems for the calculated scalar field (concentration and turbulent kinetic energy). The calculated flow variables showed nearly no difference between the second and third mesh systems. Therefore, the third mesh system with more meshes (4,000,000) was used in this study to adequately capture the buoyancy effect in a thermal environment. Figure 5 shows the mesh system used in this study. The grid number in each direction was $494 \times 109 \times 81$ ($x \times y \times z$); more meshes were used for the fourth, fifth, and sixth rows of the building blocks and the street canyons between them to ensure that the flow could be well predicted for the investigated street canyons. In addition, 16 points were used for discretizing the gas discharge line in the stream-wise direction. The depth of the first fluid cells on the floor and building surfaces was set to 120 mm. The non-dimensional distances (y^+) from the first fluid cells to the wall surfaces were less than 1000 in most regions of the building surfaces; this satisfies the requirement that y^+ should usually be in the range of 30–1000 when the logarithmic law is used. Finer meshes were adopted near the wall surfaces, and the mesh increasing rates were controlled to less than 1.25. This study investigated purely ground heating effects on ventilation and pollutant transport phenomena through this mesh system.

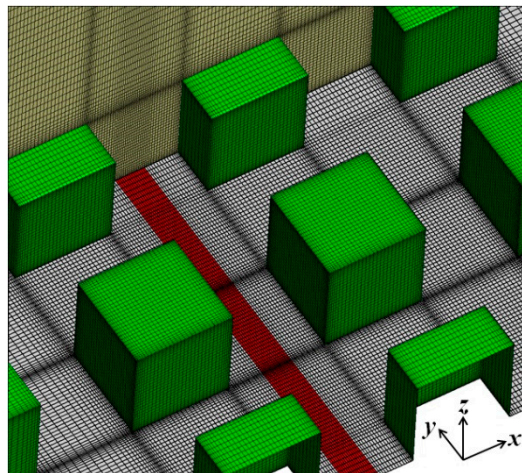


Figure 5. Computational meshes.

5. Results and Discussion

5.1. Distributions of Mean Velocity Field

Figure 6 presents the mean streamlines and normalized velocity magnitude in the symmetry plane of the TSC for different ground heating cases (GH-30, GH-40, GH-50, and GH-60). A primary recirculation was observed inside the street canyon for all ground heating cases. The core of the primary recirculation was near the roof level, and it shifted slightly to the leeward wall as ground heating increased. These flow structures are similar to the LES results reported by Nazarian and Kleissl [21] and Jiang and Yoshie [22] in the simulation of a 3D street canyon (unit aspect ratio) flow at reduced scale; however, they greatly differ from the structures of 2D street-canyon flows reported in previous studies [5,6,10–12], in which the core of the primary recirculation was located at the center of the street canyon and two additional small recirculations formed at the corners of both windward and

leeward walls at the ground level. This is a major difference between a 2D and a 3D street-canyon flow; ventilation from side surfaces may modify the flow considerably in a 3D street canyon [21,22]. As the ground temperature increased, the velocity magnitude increased significantly near the windward wall and ground level, and the area with small velocity magnitudes around the core of primary recirculation (blue area) decreased, indicating that ground heating can enhance the mean flow inside street canyons. This finding is in line with those of previous studies on 2D street-canyon flows [5,6].

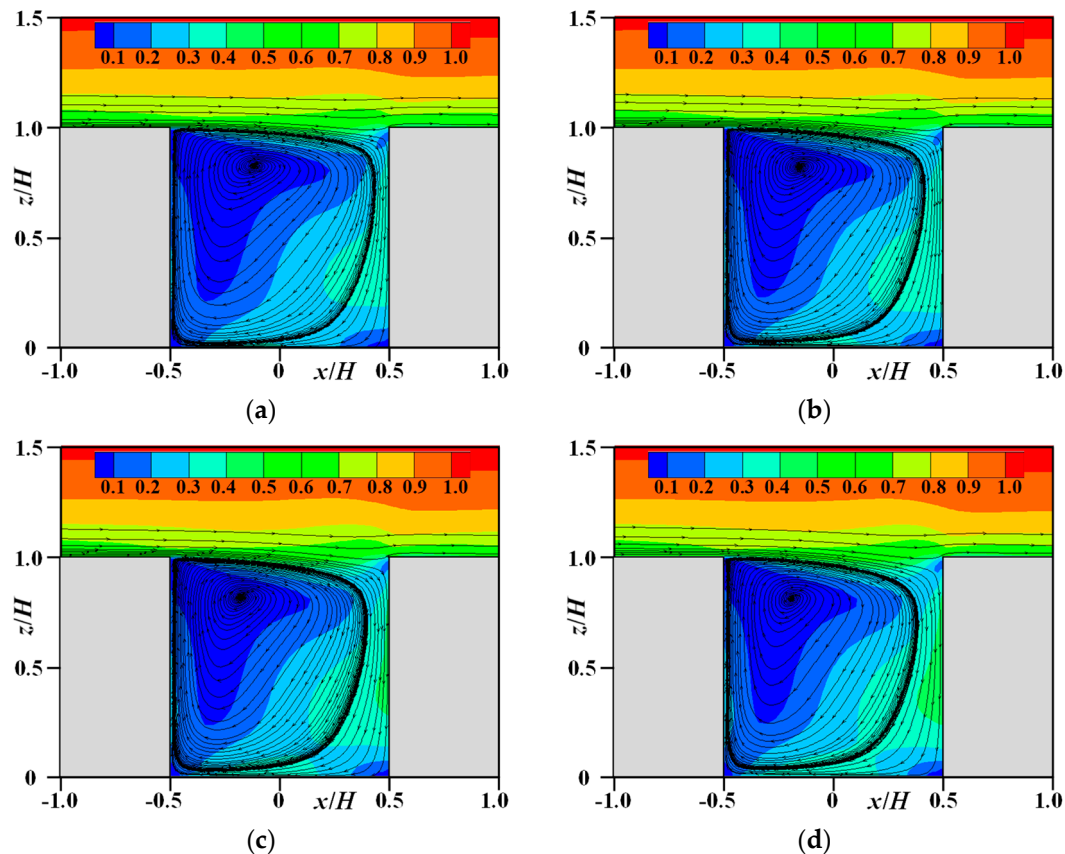


Figure 6. Mean streamlines and normalized velocity magnitude $(U^2 + V^2 + W^2)^{0.5} / U_H$ in symmetry plane ($y = 0$, target street canyon (TSC)): (a) GH-30; (b) GH-40; (c) GH-50; (d) GH-60.

Figure 7 illustrates the mean velocity vectors in a horizontal plane at half building height ($z/H = 0.5$), and in a horizontal plane at the ground level ($z/H = 0.1$) of the TSC (GH-30). From Figure 7a, when air entered the street canyon from the side surfaces, except for the small part of air leaving the street canyon at the corners, most of the air flowed toward the inner area owing to the impinging effect of the windward wall; this formed a recirculation region inside the street canyon. Air leaving the street canyon from the side surfaces is clearly illustrated in Figure 7b at the ground level; this disturbed the flow in the passageways. These flow structures are quite similar to the CFD results obtained by Kim and Baik [19] in their unsteady simulations using the RANS model. Figures 6 and 7 together clearly reveal that air entered the street canyon from the top surface and upper area of the side surfaces, and flowed out of the street canyon from the lower part of the side surfaces. Figure 8 shows the distributions of normalized mean streamwise velocity in a vertical centerline of the TSC. The experiments obtained by Uehara et al. [18] for different unstable thermal stratifications are also presented herein as references. Clear strong reverse flow was observed in the lower part of the street canyon for stronger ground heating cases in the CFD results, a tendency similar to that observed in the experiments conducted by Uehara et al. [18]. Cheng and Liu [6] derived the same conclusions in their simulations of 2D street-canyon flows. The discrepancy between the current CFD results and the experiments conducted by Uehara et al. [18] may arise from the different inflow conditions, different

scales, and different block arrangements. Another factor may be the inaccuracy of the RANS model for full-scale simulations. According to the study by Chew et al. [17], it has the possibility that the performances of the RANS models become inaccurate for full-scale simulations in some cases, such as windward wall heating.

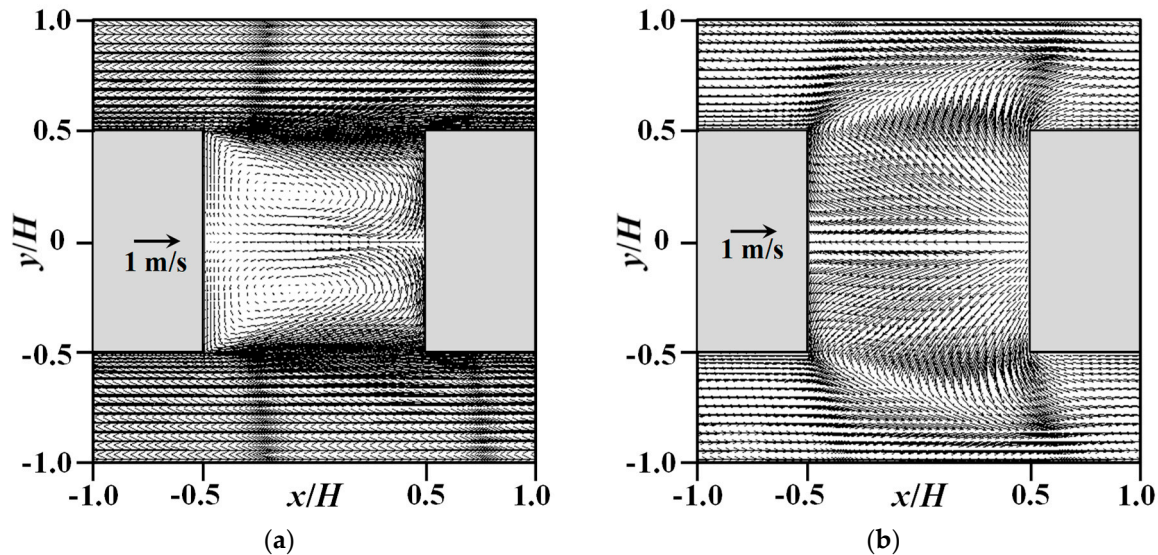


Figure 7. Mean velocity vectors in horizontal planes of the TSC (GH-30): (a) $z/H = 0.5$; (b) $z/H = 0.1$.

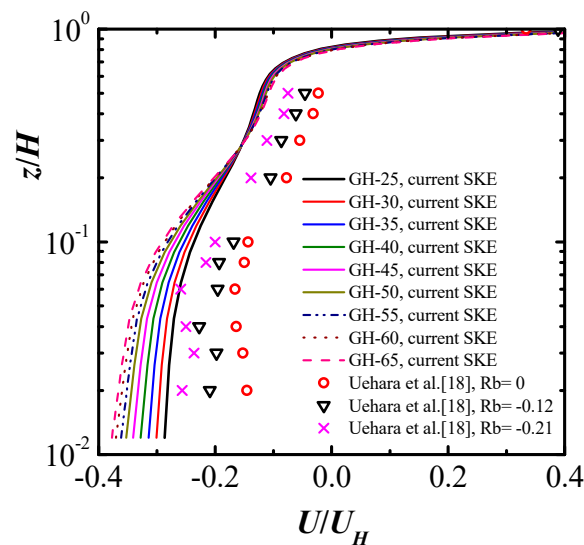


Figure 8. Distributions of normalized mean streamwise velocity along vertical centerline of the TSC.

5.2. Distributions of Pollutant Concentration

Figure 9 shows the mean streamlines and normalized concentration field in the symmetry plane of the PSC. These flow structures are quite similar to those in the TSC shown in Figure 6. The pollutant with higher concentration was blown to the leeward wall owing to recirculation inside the street canyon, and the contour lines uplifted near the leeward wall owing to rising flow. As the ground temperature increased, a decrease in pollutant concentration could be observed inside the PSC, especially at the ground level. A distinct decrease of the pollutant concentration near the top corner of the windward wall is an evidence that ground heating could promote the downward flow from the top layer. As indicated in Figure 9, the pollutant with a lower concentration existed above the roof level of the PSC. One reason is that the pollutant inside the street canyon could be transported out through the

roof level near the leeward wall owing to recirculation inside the street canyon. However, the main reason is turbulent diffusion at the roof level, as demonstrated subsequently in detail.

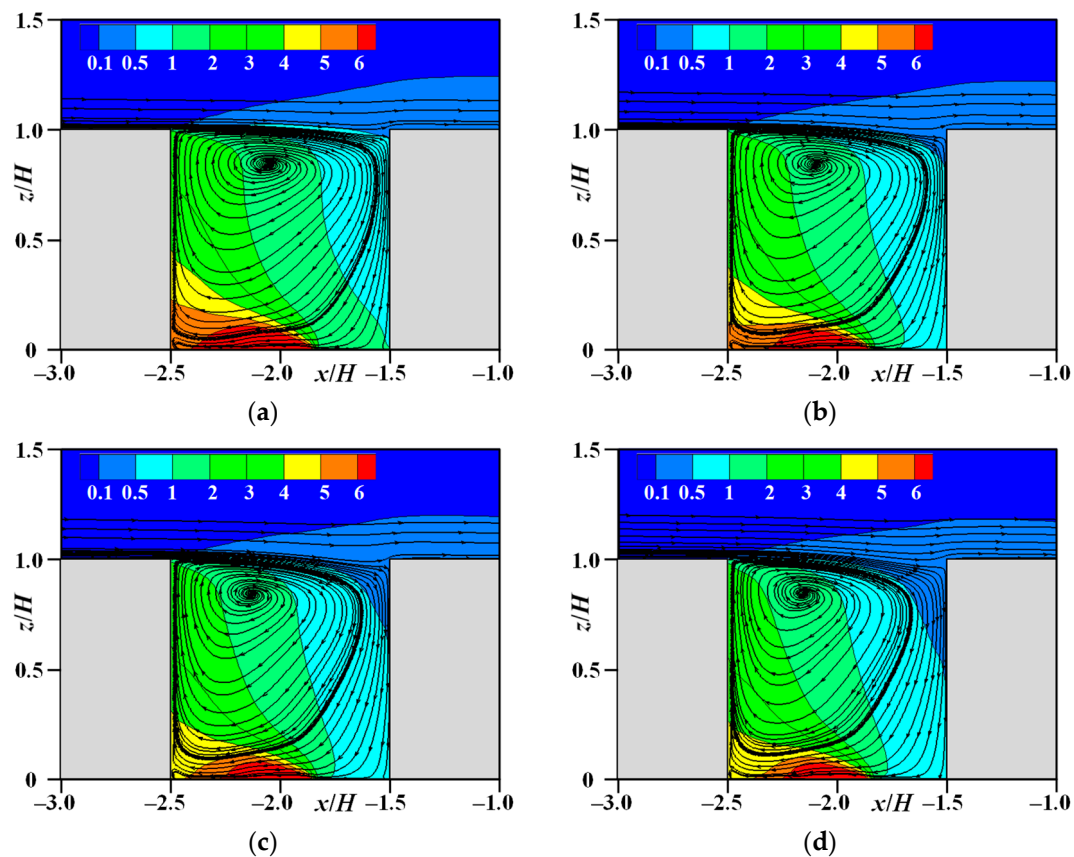


Figure 9. Mean streamlines and normalized concentration C/C_* in the symmetry plane of pollutant source canyon (PSC) ($y = 0$): (a) GH-30; (b) GH-40; (c) GH-50; (d) GH-60.

Figure 10 presents the mean velocity vectors and normalized mean concentration in a horizontal plane of the PSC near the ground ($z/H = 0.1$). Overall, these flow structures are similar to that shown in Figure 7b in the TSC; however, the flows were still slightly affected by the gas discharge line at the ground level. Owing to the reverse flow and outward flow at this ground level, a higher concentration could be observed near the leeward wall and side boundaries, whereas a lower concentration was observed near the windward wall. The concentration inside the street canyon was much higher than that in the adjacent passageways for all simulations because the pollutant with a higher concentration was blown downstream owing to high wind speed in the passageways. As the ground temperature increased, the high-concentration area near the leeward wall and side boundaries shrunk and the area with a lower concentration near the windward wall expanded considerably (blue area became larger); this is further evidence that ground heating enhances the mean flow inside a street canyon. As revealed in Figure 10, the distribution pattern of the pollutant concentration was strongly affected by the mean flow inside the street canyon. Li et al. [5] and Cheng and Liu [6] derived similar conclusions in their simulations of flow and dispersion inside 2D street canyons by using LES models, in which ground heating facilitated pollutant removal owing to the strengthening of the mean flow and turbulence inside the street canyons.

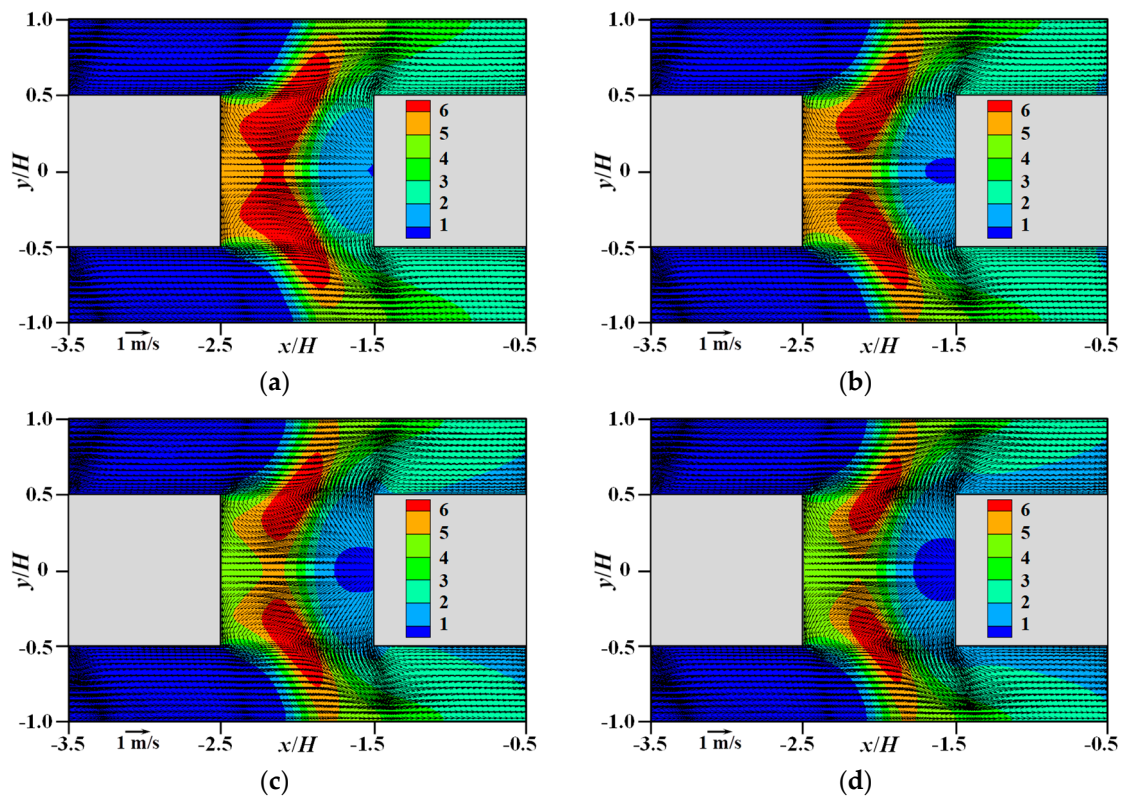


Figure 10. Mean velocity vectors and normalized concentration C/C^* in horizontal plane of the PSC ($z/H = 0.1$): (a) GH-30; (b) GH-40; (c) GH-50; (d) GH-60.

Figure 11 presents the mean velocity vectors and normalized mean concentration in the middle cross section of the TSC ($x/H = 0$). As indicated in these figures, air entered the street canyon from the top surface and the upper three quarters of the side surfaces but flowed out from the lower regions of the side surfaces, and two symmetry recirculation areas were formed in this cross section. As illustrated in Figure 11, the pollutant concentration in the two adjacent passageways was considerably higher than that inside the street canyon. Notably, most of the pollutant inside the TSC originated from the adjacent passageways, where the pollutant with a higher concentration originated from the line pollutant source upstream (see Figure 10) because no pollutant source existed inside the TSC. Although a pollutant existed above the roof and could be transported into the street canyon through the mean air flow, no pollutant could actually enter the street canyon from the top surface owing to the pollutant outflow rate contributed by turbulent diffusion, as explained in a subsequent section. Weaker velocities were observed near the top surface but stronger velocities were observed at the side surfaces, especially in their lower regions, indicating that air convection dominated pollutant transport at side surfaces but did not contribute much at the top surface. Although not distinct, the length of the velocity arrows gradually increased with the ground temperature, signifying that ground heating could enhance the mean flow inside the street canyon. As shown in Figure 11, the higher concentration area decreased and the lower concentration area expanded inside the street canyon as the ground temperature increased; in this figure, the shape of the contour line of 0.1 above the roof level changes from convex for the case of lower ground heating to concave for the case of higher ground heating. Notably, although the inflow air from the top surface had a lower velocity, its circulation path was much longer than that of the inflow air from the side surfaces. In addition, a large ventilation channel was observed in the middle area of the street canyon; this channel nearly coincided with the lower concentration area.

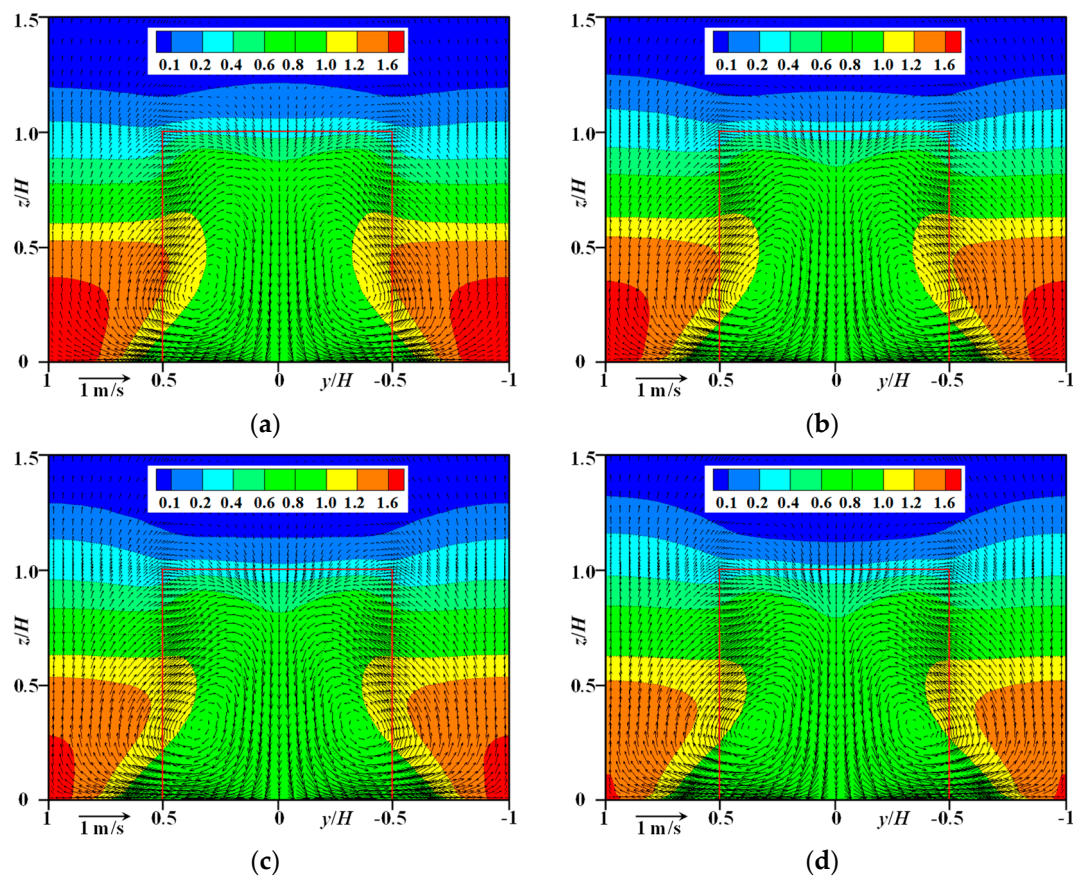


Figure 11. Mean velocity vectors and normalized concentration C/C^* in middle cross section of the TSC ($x/H = 0$): (a) GH-30; (b) GH-40; (c) GH-50; (d) GH-60.

To further examine the effect of ground heating on the concentration field, plane averaged scalar fields (turbulent kinetic energy and mean concentration) in the TSC were assessed, as shown in Figure 12. Along the vertical direction, 10 horizontal cross sections were generated per meter, and the scalar fields were averaged in each section according to the following equation:

$$k_{ave} = \frac{\sum k_j A_j}{A}, C_{ave} = \frac{\sum C_j A_j}{A} \tag{13}$$

where A is the total area in each section ($= H^2$ in this study). As presented in Figure 12, as the ground temperature increased, the plane-averaged turbulent kinetic energy increased significantly and the plane averaged pollutant concentration decreased in all sections. Considering the entire TSC as a control volume, we could observe that ground heating could enhance turbulence and promote pollutant reduction inside the street canyon. An inversely proportional relationship seemed to exist for the turbulent kinetic energy and the mean concentration inside the street canyon. This is why most studies have stressed the effects of turbulence for pollutant removal when ground heating intensifies [5,6].

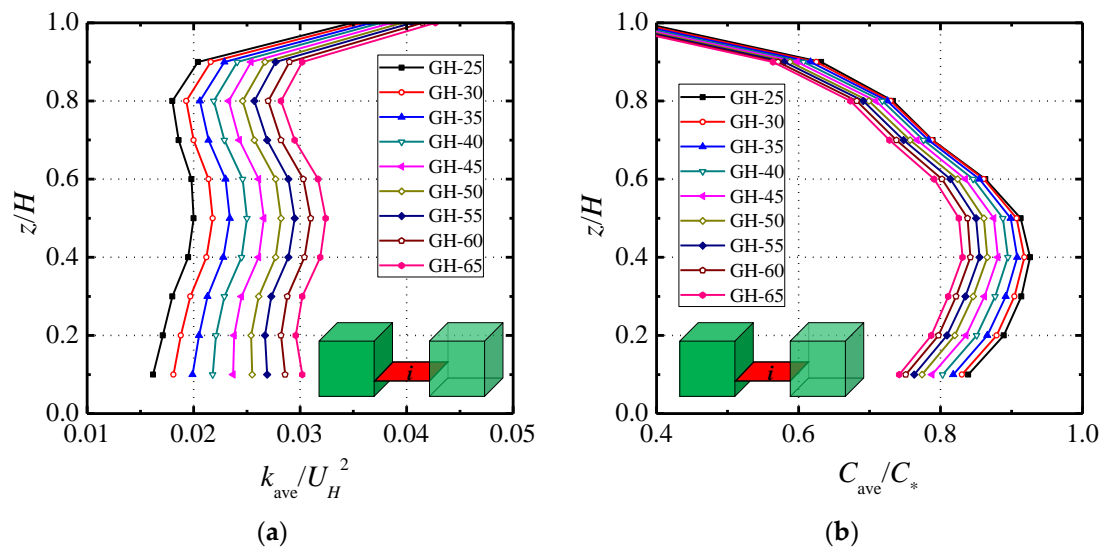


Figure 12. Plane-averaged scalar fields in the TSC: (a) plane-averaged turbulent kinetic energy; (b) plane-averaged pollutant concentration.

Figure 13 presents normalized pollutant fluxes of normal direction at the three boundaries of the TSC. Only the case GH-30 is shown here; the distribution patterns in the other cases were quite similar to that in this case. The convective flux has the same sign as the mean velocity perpendicular to the boundary. The convective flux WC was negative in most areas of the top surface, indicating that the pollutant was transported into the street canyon by air convection in these regions. Small areas with positive WC values could also be observed near the leeward and windward walls owing to air outflow in these regions. Positive turbulent diffusion flux $\langle w'c' \rangle$ throughout the top surface indicated that the sole effect of turbulence was to remove the pollutant from the street canyon at this surface. The same conclusions have also been obtained by Cheng and Liu [6] in their simulations of a 2D street-canyon flow and by Jiang and Yoshie [22] in a 3D urban flow simulation. The positive $\langle w'c' \rangle$ value was larger than the negative WC value at the top surface, leading to a positive value of the total pollutant flux $\langle wc \rangle$ throughout the top surface. This means that for the averaging effect, the pollutant was transported out from entire top surface and the pollutant did not enter the street canyon from the top surface, although the concentration was not zero above the roof. As indicated in Figure 13a, the pollutant was transported into street canyon from the passageways by air convection in nearly three-quarters of the upper side surfaces; this is consistent with that shown in Figure 11. The pollutant was transported out by air convection through the lower regions of the side surfaces. As shown in Figure 13b, the area with negative values of turbulent diffusion flux $\langle v'c' \rangle$ was mainly located in the lower half regions of the left surface. According to the gradient diffusion hypothesis of Equation (3), we can conclude that the negative $\langle v'c' \rangle$ values at the left surface imply a positive gradient of the mean concentration in these regions; therefore, the pollutant concentration in the passageways was higher than that inside the street canyon. Because the magnitude of VC was much larger than $\langle v'c' \rangle$ at the side surfaces, the distribution pattern of the total pollutant flux $\langle vc \rangle$ became more similar to that of the convective flux VC ; therefore, air convection dominated the pollutant transport at the side surfaces.

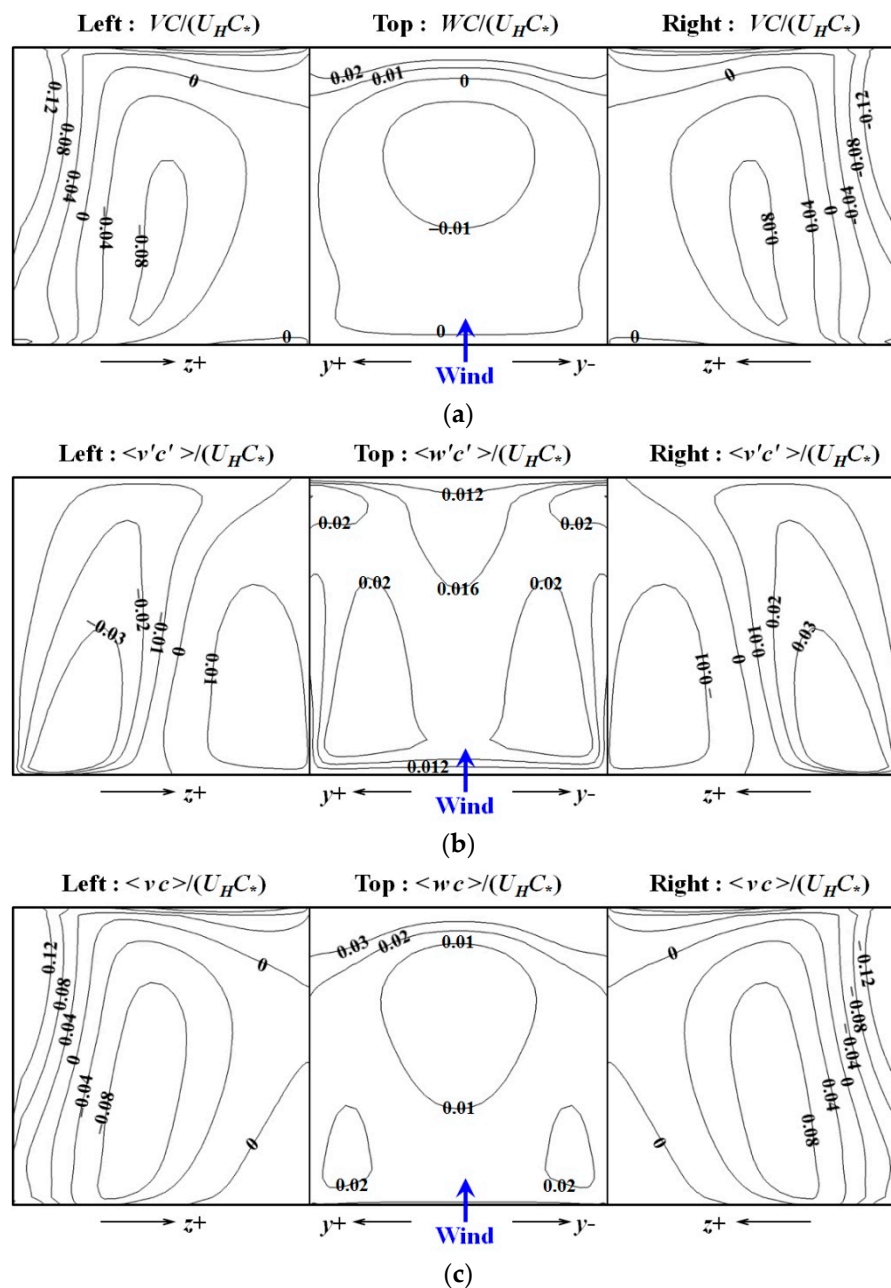


Figure 13. Normalized pollutant fluxes in normal direction at boundaries of the TSC (GH-30): (a) convective flux; (b) turbulent diffusion flux; (c) total pollutant flux.

5.3. Pollutant and Air Flow Rate Analysis

This section investigated the ventilation and pollutant transport processes between a 3D street canyon and an outer environment by analyzing air and pollutant flow rates at the boundaries. Figure 14a,b illustrate the contributions of air convection and turbulent diffusion to pollutant flow rates at the boundaries of the PSC for case GH-30 (flow rates for two side surfaces were combined). The green and red bars in the figures indicate the contributions by air convection and turbulent diffusion, respectively. The pollutant discharge rate q_p was used to normalize the pollutant flow rates. The contribution percentages of turbulent diffusion (red bar/total bar) are also marked. For the PSC, turbulent diffusion dominated pollutant outflow at all boundaries; however, it did not contribute to pollutant inflow at the top surface. This is consistent with the conclusions obtained by Liu and Wong [4] and Cheng and Liu [6] in their studies on 2D street-canyon flows, in which pollutant removal

from the street canyons to the prevailing flow was mainly governed by turbulence and the vertical turbulent diffusion flux $\langle w'c' \rangle$ was positive throughout the roof level. The major reason for the dominant contribution of turbulent diffusion is that the PSC included pollutant source and that the discharged pollutant was mixed and transported to the entire street canyon from the ground level due to recirculation and turbulence inside the street canyon; this thus resulted in a considerably higher pollutant concentration inside the street canyon than those in the surrounding space. According to Equation (3), a larger gradient of mean concentration beside the boundaries of a street canyon would lead to a larger contribution of turbulent diffusion to pollutant outflow. Turbulent diffusion also contributed a little to pollutant inflow rate (Figure 14a) in small area of the side surfaces, this small area was mainly located near the windward wall at the ground level. This could be observed in Figure 10a, which reveals a lower pollutant concentration near the windward wall inside the PSC. According to the different ranges of vertical coordinates in Figure 14a,b, the pollutant outflow rates were much larger than the pollutant inflow rates at both side surfaces and the top surface of the PSC; this can primarily be attributed to the existence of the pollutant source. Figure 14c,d show the contributions of air convection and turbulent diffusion to pollutant flow rates at the boundaries of the TSC for case GH-30. For the TSC, the pollutant inflow rate was larger than the outflow rate at the side surfaces; however, the opposite was true for the top surface. Air convection dominated pollutant transport at the side surfaces, and its contribution to both pollutant inflow and outflow rates could be observed at the top surface. Turbulent diffusion considerably contributed to the pollutant inflow rate at the side surfaces and dominated pollutant outflow at the top surface. However, it did not contribution to the pollutant inflow rate at the top surface. These pollutant transport behaviors at the boundaries of the TSC are quite similar to that reported by Jiang and Yoshie [22] in the studies of pollutant transport in a reduced-scale 3D urban environment through LES; nevertheless, small differences could be found between the two studies. For the pollutant outflow rates presented in Figure 14d, the total amount at the side surfaces (red + green) was obviously higher than that at the top surface; only a slightly larger value was observed in previous research [22]. At the top surface, contribution of air convection to the pollutant inflow rate was slightly larger than that to the pollutant outflow rate in the current study, and the latter was slightly larger than the former in the previous study [22]. Whether these small differences arise from the effect of different scales or inaccuracy of the RANS model when used in full-scale simulations is unclear. Comparing Figure 14a,b with Figure 14c,d could also reveal differences. Except for the amount of transported pollutant, the main difference in pollutant transport patterns between the PSC and the TSC was that at the side surfaces, the pollutant outflow was dominated by turbulent diffusion for the PSC whereas it was dominated by air convection for the TSC.

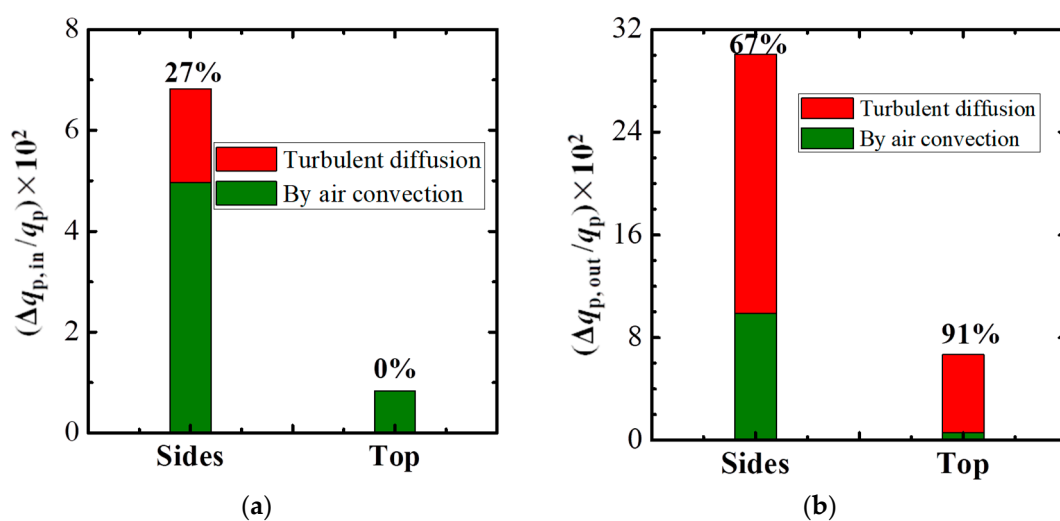


Figure 14. Cont.

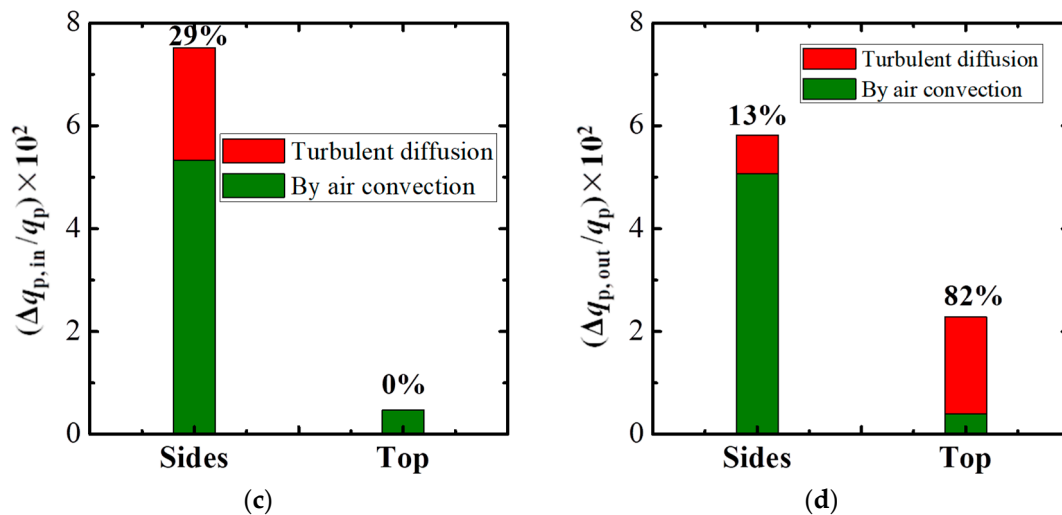


Figure 14. Contributions of air convection and turbulent diffusion to pollutant flow rates at the boundaries of the PSC and TSC (GH-30): (a) pollutant inflow rates (PSC); (b) pollutant outflow rates (PSC); (c) pollutant inflow rates (TSC); (d) pollutant outflow rates (TSC). (The percentages in the Figures mean the red bar/total bar).

Obvious difference in pollutant transport behavior between the PSC and the TSC could be observed from the analysis of total pollutant flow rates, as illustrated in Figure 15 (case GH-30), where the blue and pink bars indicate inflow and outflow, respectively. For the PSC, the total pollutant inflow rate was zero at the top surface and nearly zero at the side surfaces. This signifies that for pseudo-steady flow, the pollutant was discharged from the ground level inside the PSC and was removed through all boundary surfaces. For the TSC, the pollutant entered the street canyon from the side surfaces and most of it left from the side surfaces and some left from the top surface. Zero total pollutant inflow rate at the top surface implies that no pollutant entered the street canyon from the top surface, and the only role of the top surface was to remove the pollutant. This is in line with the result presented in Figure 13c, which shows that the total pollutant flux $\langle wc \rangle$ was positive throughout the top surface of the TSC. The total amount of transported pollutant in the PSC was much larger than that in the TSC because of the existence of pollutant source in the PSC. Solving the pollutant transport equation means that the pollutant mass is conserved in each cell of the mesh system. If the entire street canyon is considered a control volume, the pollutant mass should be conserved inside the street canyon. As shown in Figure 15b, the amount of pollutant entering the street canyon (blue bar at side surfaces) is just equal to the amount of pollutant leaving the street canyon (pink bar at side surfaces plus pink bar at top surface); therefore, the pollutant mass is adequately balanced. As illustrated in Figure 15, compared with the PSC, the pollutant transport process is more complicated for the TSC, because both pollutant inflow and outflow could be observed at the side surfaces.

Figure 16 displays the contributions of air convection and turbulent diffusion to pollutant flow rates at the boundaries of the TSC as the ground temperature increased. As presented in Figure 16a, as the ground temperature increased, the contributions of air convection to both pollutant inflow and outflow rates increased significantly at the side surfaces; this can primarily be attributed to the enhancement of ventilation at the side surfaces. At the top surface, the contributions of air convection to both pollutant inflow and outflow rates exhibited slight changes as the ground heating intensity increased. The contributions of air convection to pollutant inflow rates were a little larger than those to pollutant outflow rates at both the side and top surfaces. As illustrated in Figure 16b, as the ground temperature increased, the contributions of turbulent diffusion to both pollutant inflow rates (black line) and outflow rates (red line) slightly decrease at the side surfaces, and the decreasing speed of the red line was a little faster. At the top surface, the contributions of turbulent diffusion to pollutant inflow rates were zero for all cases, and those to pollutant outflow rates gradually increased with the

ground temperature, indicating that the sole effect of turbulent diffusion was to remove the pollutant from the street canyon at the top surface. A comparison of Figure 16a,b could reveal that air convection dominated pollutant transport (both inflow and outflow) at side surfaces; however, turbulent diffusion dominated pollutant transport at the top surface, mainly to pollutant outflow. Because of recirculation inside the street canyon, the pollutant with a higher concentration could not be easily transported out through the top surface by air convection; consequently, turbulent diffusion dominated pollutant removal at the roof level.

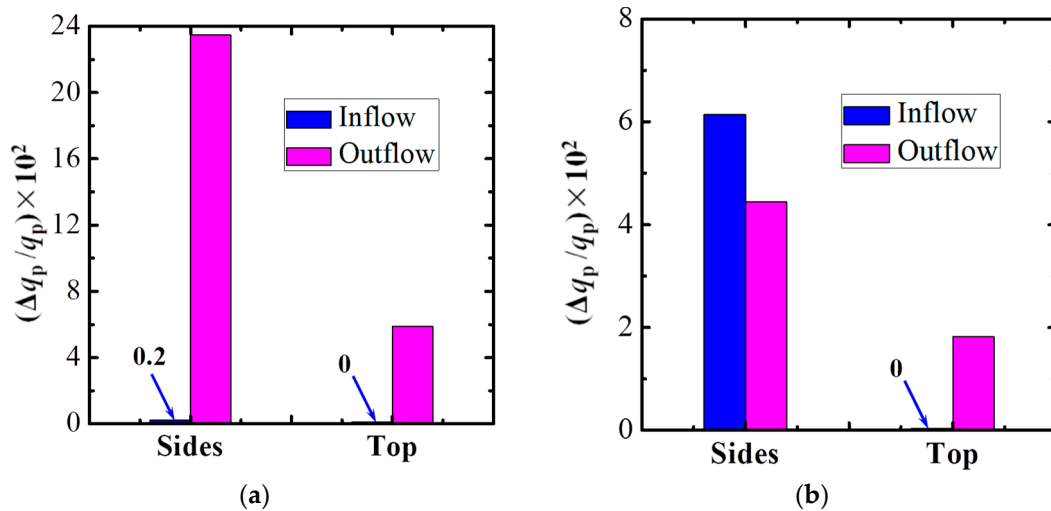


Figure 15. Total pollutant flow rates at the boundaries of the PSC and TSC (GH-30): (a) PSC; (b) TSC.

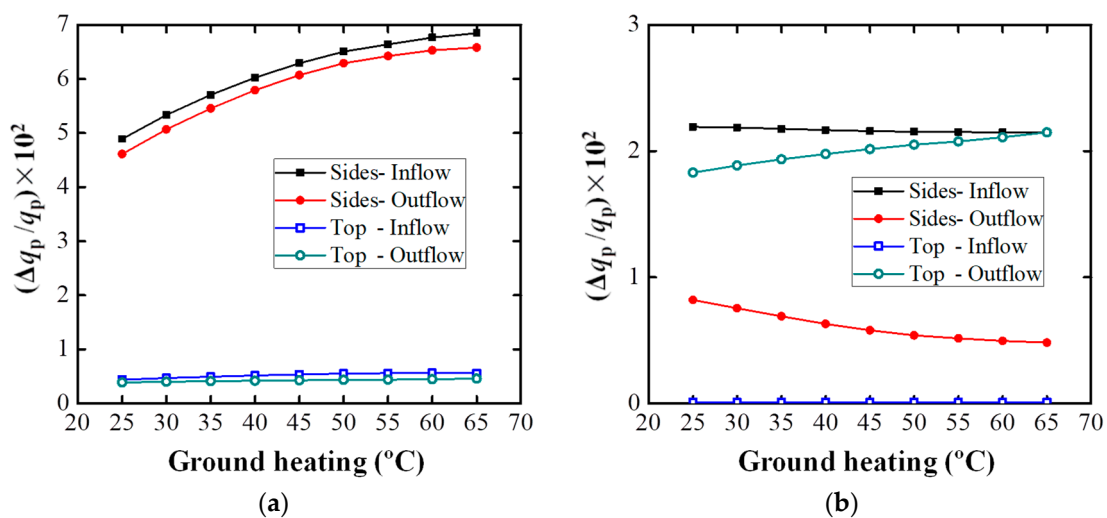


Figure 16. Contributions of air convection and turbulent diffusion to pollutant flow rates with ground heating (TSC): (a) contributions by air convection; (b) contributions by turbulent diffusion.

Figure 17 shows the changes in total pollutant flow rates and air flow rates at the boundaries of the TSC as the ground temperature increased. $q_a = \rho U_H H^2$ was used to normalize the air flow rates. As revealed in Figure 17a, both the total pollutant inflow and outflow rates increased significantly at the side surfaces when the ground temperature increased; consequently, ground heating could promote pollutant exchange at the side surfaces. The total pollutant inflow rates were zero at the top surface for all cases, and the total pollutant outflow rate increased slightly as the ground temperature increased. Because of the conservation of the pollutant mass, the total pollutant inflow rates should equal the total pollutant outflow rates at the boundaries of the TSC for all the cases. Accordingly, a slight increase in total pollutant outflow rates at the top surface implies that the increase of the total pollutant inflow rate should be larger than that of the total pollutant outflow rate at the side surfaces

(vertical distance between black and red lines should increase). Consequently, more pollutant would be brought to the street canyon from the side surfaces when ground temperature increased. As the ground heating intensity increased, significant increases in both air inflow and outflow rates could be observed for the side surfaces, as presented in Figure 17b. However, the increase in the air outflow rate was greater than that in the inflow rate at the side surface. An obvious increase in the air inflow rate could also be observed at the top surface; however, the changes in the air outflow rate at the top surface were quite small. If we consider the entire inner space of the TSC as a control volume, mass conservation of air should be satisfied as the continuity equation was solved in the CFD simulations. This means that the total air inflow rates should equal the total air outflow rates at the boundaries of the TSC. The mass balance of air can be adequately reflected in the variation tendencies of air flow rates shown in Figure 17b. The increasing air inflow rates at both the side and top surfaces indicate that the ventilation was enhanced by the ground heating. As displayed in Figure 17, the amounts of pollutant and air exchanged at the side surfaces were much larger than those at the top surface. Therefore, air and pollutant exchanges between the TSC and the outer space occurred primarily through the side surfaces.

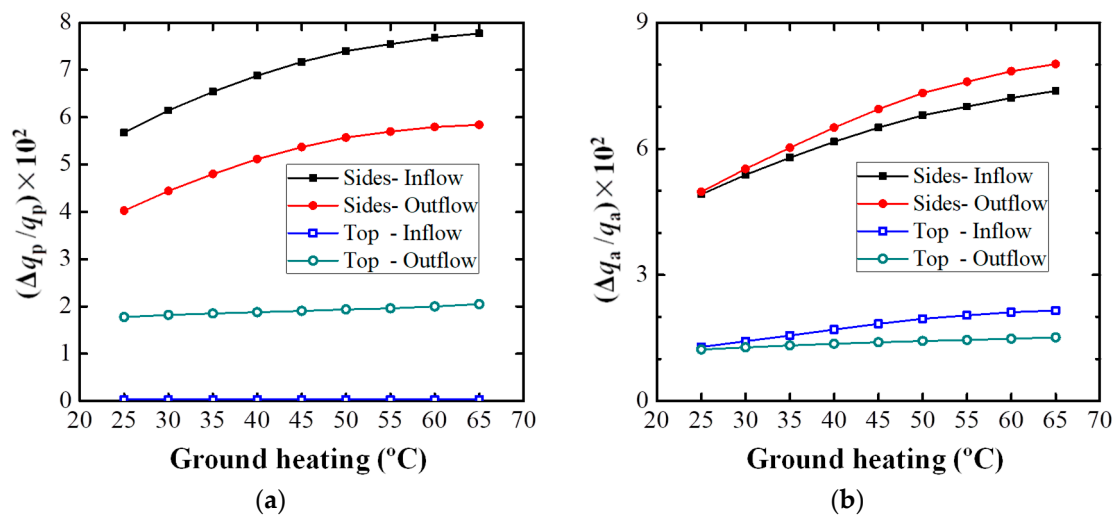


Figure 17. Changes in total pollutant flow rates and air flow rates with ground heating (TSC): (a) total pollutant flow rates; (b) air flow rates.

As discussed in this study, as the ground temperature increases, the pollutant concentration inside the street canyons decreased significantly. This finding can be attributed to many factors. From the distributions of the plane-averaged scalar fields in the TSC as presented in Figure 12, larger turbulent kinetic energy and smaller pollutant concentration could be clearly observed at each height for strong ground heating cases, and indeed the negative relationship between the two variables was observed. This may be why turbulence was considered one of the most important factors responsible for pollutant reduction inside the street canyon. Although stronger turbulence can promote pollutant mixing inside a street canyon, it may also cause pollutant reduction at local stations. However, in this study, we could not find direct evidence that the enhanced turbulence contributes to pollutant reduction for the whole TSC. When the ground temperature increases, some beneficial factors for pollutant removal from the street canyon could be observed in Figure 16, such as air convection at the side surfaces and turbulent diffusion at the top surface. However, explaining pollutant reduction phenomena from the viewpoint of pollutant removal is still difficult. Because the pollutant mass is always balanced inside a street canyon for steady flow, if more pollutant is removed from the street canyon, then more pollutant will enter the street canyon. An analysis of both total pollutant flow rates and air flow rates in combination can help clarify this issue.

As displayed in Figure 17a, the increase of the total pollutant inflow rate is slightly larger than that of the total pollutant outflow rate at the side surfaces. Consequently, more pollutant was brought into the street canyon from the side surfaces when the ground temperature increased; the side surfaces thus exhibited a negative effect and were not responsible for pollutant reduction inside the street canyon with ground heating. Increasing air inflow rates from the top surface are clearly the most likely reasons for pollutant reduction inside the TSC. This is because compared with the polluted air inside the street canyon, the air above the top surface was fresher. For an incompressible flow, the total mass (including air and pollutant) that could be contained in a street canyon is already fixed. When more fresh air enters the street canyon from the top surface, more space inside the street canyon is occupied by fresh air, and the enhanced mean flow and turbulence by ground heating promote mixing. The pollutant inside the street canyon is thus diluted. Accordingly, for the TSC, although air/pollutant exchange between the street canyon and the outer space mainly occurred through the side surfaces and the exchanged air and pollutant were small at the top surface, the increase in air inflow from the top surface contributed most to pollutant reduction inside the street canyon when the ground temperature increased. Except for increased air inflow rates, other results supporting the key role of the top surface in pollutant reduction are outlined as follows: the circulation path of inflow air from the top surface was much longer (Figure 11), no pollutant entered the street canyon from the top surface for all ground heating cases (Figure 17a), and the total pollutant outflow rate increased slightly at the top surface when the ground temperature increased (Figure 17a).

6. Conclusions

In this study, a validated SKE model was used to investigate the effects of ground heating on ventilation and pollutant transport in a 3D environment. Pollutant transport behavior was investigated for both a street canyon that included a pollutant source (PSC) and a target street canyon downstream (TSC), and the complicated transport processes in the TSC were studied in detail. As the ground temperature increased, contributions of air convection and turbulent diffusion to pollutant transport were determined, and the reasons why the pollutant concentration inside the street canyon changes were discussed.

This study observed 3D recirculation in a 3D street-canyon flow. Air entered the street canyon from the top surface and upper area of the side surfaces and exited the canyon from the lower part of the side surfaces. Compared with the reported 2D street-canyon flows, the core of primary recirculation was near the top surface in this study, signifying that side ventilation modifies the flow significantly. Ground heating can enhance the mean flow and turbulence inside the street canyon, and promote pollutant reduction. This is in line with the findings of previous studies on a 2D street-canyon flow and dispersion.

Different pollutant transport behaviors for the PSC and the TSC were studied through the analysis of the pollutant fluxes and pollutant flow rates at the boundaries. The pollutant did not enter the PSC, and turbulent diffusion dominated pollutant outflow at all boundaries. The pollutant entered the TSC from the upper three-quarter areas of the side surfaces and exited from the entire top surface and lower regions of the side surfaces. Air convection dominated pollutant transport (both inflow and outflow) at the side surfaces, and its contributions increased significantly as the ground temperature increased; turbulent diffusion dominated pollutant transport at the top surface, but only to pollutant outflow, and its contribution increased slightly when the ground heating intensity increased.

The main factors causing pollutant reduction inside the TSC were further examined by analyzing both the total pollutant flow rates and air flow rates. When the ground temperature increased, both the air inflow and outflow rates increased significantly at the side surfaces, an obvious increase of air inflow rate could also be observed at the top surface; consequently, ground heating enhanced ventilation for the street canyon. When the ground temperature increased, both the total pollutant inflow and outflow rates increased significantly at the side surfaces, but the increase of the former one is a little faster than the latter one, indicating that the side surfaces had a negative effect and made no

contribution to pollutant reduction inside the street canyon. The increase in air inflow rate from top surface was considered to be responsible for pollutant reduction inside the street canyon when the ground temperature increased, because the increasing fresh air from the top surface occupied more inner space of the street canyon; then, the enhanced mean flow and turbulence promoted mixing and thereby the polluted air inside the street canyon was diluted. Therefore, the top surface played a major role in pollutant reduction/dilution inside the street canyon, although air and pollutant exchanges between the street canyon and surrounding environment occurred primarily through the side surfaces.

This study investigated the effect of ground heating on basic pollutant transport phenomena through an idealized 3D street canyon model, and the most important reasons that affect the pollutant variation inside a 3D street canyon was determined as ground heating. These can supply valuable suggestions to improve the air quality for the urban planning strategies. The pollutant transport phenomenon was studied by the analysis of the pollutant flow rates conjunction with the pollutant fluxes. The pollutant flow rates were analyzed by three methods in this research: total pollutant flow rates, pollutant flow rates contributed by air convection and turbulent diffusion. The analyzing method used in this study is quite helpful for pollutant transport investigations in urban areas. This study had its limitations suggesting future work. This study investigated purely the ground heating effect on ventilation and pollutant transport phenomena. But this phenomenon can be affected by many factors in a 3D environment, such as the aspect ratio, building facade/roof heating, and even the passage width between columns [32]. As discussed in this study, pollutant transport process in a 3D thermal environment is quite complicated, and investigating all influencing factors in one study alone is difficult. Therefore, additional studies on the effect of other factors are necessary. Currently, it remains difficult to simulate a 3D urban flow and dispersion using LES even at reduced scale when there are more building blocks; therefore, the RANS model was used in this study. Although the adopted RANS model has been evaluated through a reduced-scale experiment, uncertainty may still exist in a full-scale simulation when the buoyancy effect exists.

Author Contributions: Conceptualization, G.J. and T.H.; Formal analysis, G.J., T.H. and H.Y.; Funding acquisition, G.J. and T.H.; Investigation, G.J. and H.Y.; Methodology, G.J. and T.H.; Project administration, G.J.; Writing—original draft, G.J.; Writing—review and editing, T.H.

Funding: This research was funded by the Science and Technology Planning Project of Guangdong Province, China, grant number 2013B020200015 and the National Natural Science Foundation of China, grant number 51508395.

Conflicts of Interest: The authors declare no conflict of interest.

References

1. Oke, T.R. Street design and urban canopy layer climate. *Energ. Build.* **1988**, *11*, 103–113. [[CrossRef](#)]
2. Liu, C.H.; Cheng, W.C.; Leung, T.C.Y.; Leung, D.Y.C. On the mechanism of air pollutant re-entrainment in two-dimensional idealized street canyons. *Atmos. Environ.* **2011**, *45*, 4763–4769. [[CrossRef](#)]
3. Liu, C.H.; Leung, D.Y.C.; Barth, M.C. On the prediction of air and pollutant exchange rates in street canyons of different aspect ratios using large-eddy simulation. *Atmos. Environ.* **2005**, *39*, 1567–1574. [[CrossRef](#)]
4. Liu, C.H.; Wong, C.C.C. On the pollutant removal, dispersion, and entrainment over two-dimensional idealized street canyons. *Atmos. Res.* **2014**, *135–136*, 128–142. [[CrossRef](#)]
5. Li, X.X.; Britter, R.E.; Koh, T.Y.; Norford, L.K.; Liu, C.H.; Entekhabi, D.; Leung, D.Y.C. Large-eddy simulation of flow and pollutant transport in urban street canyons with ground heating. *Boundary Layer Meteorol.* **2010**, *137*, 187–204. [[CrossRef](#)]
6. Cheng, W.C.; Liu, C.H. Large-eddy simulation of turbulent transports in urban street canyons in different thermal stabilities. *J. Wind Eng. Ind. Aerod.* **2011**, *99*, 434–442. [[CrossRef](#)]
7. Xie, X.M.; Liu, C.H.; Leung, D.Y.C.; Leung, M.K.H. Characteristics of air exchange in a street canyon with ground heating. *Atmos. Environ.* **2006**, *40*, 6396–6409. [[CrossRef](#)]
8. Cheng, W.C.; Liu, C.H.; Leung, D.Y.C. On the correlation of air and pollutant exchange for street canyons in combined wind-buoyancy-driven flow. *Atmos. Environ.* **2009**, *43*, 3682–3690. [[CrossRef](#)]

9. Allegrini, J.; Dorer, V.; Carmeliet, J. Wind tunnel measurements of buoyant flows in street canyons. *Build. Environ.* **2013**, *59*, 315–326. [[CrossRef](#)]
10. Kim, J.J.; Baik, J.J. Urban street-canyon flows with bottom heating. *Atmos. Environ.* **2001**, *35*, 3395–3404. [[CrossRef](#)]
11. Li, X.X.; Britter, R.E.; Norford, L.K.; Koh, T.Y.; Entekhabi, D. Flow and pollutant transport in urban street canyons of different aspect ratios with ground heating: Large-eddy simulation. *Boundary Layer Meteorol.* **2012**, *142*, 289–304. [[CrossRef](#)]
12. Xie, X.M.; Liu, C.H.; Leung, D.Y.C. Impact of building facades and ground heating on wind flow and pollutant transport in street canyons. *Atmos. Environ.* **2007**, *41*, 9030–9049. [[CrossRef](#)]
13. Chatzimichailidis, A.E.; Argyropoulos, C.D.; Assael, M.J.; Kakosimos, K.E. Qualitative and quantitative investigation of multiple large eddy simulation aspects for pollutant dispersion in street canyons using OpenFOAM. *Atmosphere* **2019**, *10*, 17. [[CrossRef](#)]
14. Tominaga, Y.; Stathopoulos, T. CFD modeling of pollution dispersion in a street canyon: Comparison between LES and RANS. *J. Wind Eng. Ind. Aerod.* **2011**, *99*, 340–348. [[CrossRef](#)]
15. Dai, Y.; Mak, C.M.; Ai, Z.T.; Hang, J. Evaluation of computational and physical parameters influencing CFD simulations of pollutant dispersion in building arrays. *Build. Environ.* **2018**, *137*, 90–107. [[CrossRef](#)]
16. Yoshie, R.; Jiang, G.Y.; Shirasawa, T.; Chung, J. CFD simulations of gas dispersion around high-rise building in non-isothermal boundary layer. *J. Wind Eng. Ind. Aerod.* **2011**, *99*, 279–288. [[CrossRef](#)]
17. Chew, L.W.; Glicksman, L.R.; Norford, L.K. Buoyant flows in street canyons: Comparison of RANS and LES at reduced and full scales. *Build. Environ.* **2018**, *146*, 77–87. [[CrossRef](#)]
18. Uehara, K.; Murakami, S.; Oikawa, S.; Wakamatsu, S. Wind tunnel experiments on how thermal stratification affects flow in and above urban street canyons. *Atmos. Environ.* **2000**, *34*, 1553–1562. [[CrossRef](#)]
19. Kim, J.J.; Baik, J.J. Effects of street-bottom and building-roof heating on flow in three-dimensional street canyons. *Adv. Atmos. Sci.* **2010**, *27*, 513–527. [[CrossRef](#)]
20. Allegrini, J. A wind tunnel study on three-dimensional buoyant flows in street canyons with different roof shapes and building lengths. *Build. Environ.* **2018**, *143*, 71–88. [[CrossRef](#)]
21. Nazarian, N.; Kleissl, J. Realistic solar heating in urban areas: Air exchange and street-canyon ventilation. *Build. Environ.* **2016**, *95*, 75–93. [[CrossRef](#)]
22. Jiang, G.Y.; Yoshie, R. Large-eddy simulation of flow and pollutant dispersion in a 3D urban street model located in an unstable boundary layer. *Build. Environ.* **2018**, *142*, 47–57. [[CrossRef](#)]
23. Tominaga, Y.; Stathopoulos, T. CFD modeling of pollution dispersion in building array: Evaluation of turbulent scalar flux modeling in RANS model using LES results. *J. Wind Eng. Ind. Aerod.* **2012**, *104–106*, 484–491. [[CrossRef](#)]
24. Gousseau, P.; Blocken, B.; Stathopoulos, T.; van Heijst, G.J.F. Near-field pollutant dispersion in an actual urban area: Analysis of the mass transport mechanism by high-resolution Large Eddy Simulations. *Comput. Fluids* **2015**, *114*, 151–162. [[CrossRef](#)]
25. Xie, X.M.; Huang, Z.; Wang, J.S. Impact of building configuration on air quality in street canyon. *Atmos. Environ.* **2005**, *39*, 4519–4530. [[CrossRef](#)]
26. Mochida, A.; Tominaga, Y.; Murakami, S.; Yoshie, R.; Ishihara, T.; Ooka, R. Comparison of various $k-\epsilon$ models and DSM applied to flow around a high-rise building - report on AIJ cooperative project for CFD prediction of wind environment. *Wind Struct.* **2002**, *5*, 227–244. [[CrossRef](#)]
27. Tominaga, Y.; Mochida, A.; Murakami, S.; Sawaki, S. Comparison of various revised $k-\epsilon$ models and LES applied to flow around a high-rise building model with 1:1:2 shape placed within the surface boundary layer. *J. Wind Eng. Ind. Aerod.* **2008**, *96*, 389–411. [[CrossRef](#)]
28. Yoshie, R.; Mochida, A.; Tominaga, Y.; Kataoka, H.; Harimoto, K.; Nozu, T.; Shirasawa, T. Cooperative project for CFD prediction of pedestrian wind environment in the Architectural Institute of Japan. *J. Wind Eng. Ind. Aerod.* **2007**, *95*, 1551–1578. [[CrossRef](#)]
29. Tominaga, Y.; Stathopoulos, T. Turbulent Schmidt numbers for CFD analysis with various types of flow field. *Atmos. Environ.* **2007**, *41*, 8091–8099. [[CrossRef](#)]
30. Tominaga, Y.; Mochida, A.; Yoshie, R.; Kataoka, H.; Nozu, T.; Yoshikawa, M.; Shirasawa, T. AIJ guidelines for practical applications of CFD to pedestrian wind environment around buildings. *J. Wind Eng. Ind. Aerod.* **2008**, *96*, 1749–1761. [[CrossRef](#)]

31. Niachou, K.; Livada, I.; Santamouris, M. Experimental study of temperature and airflow distribution inside an urban street canyon during hot summer weather conditions—Part I: Air and surface temperatures. *Build. Environ.* **2008**, *43*, 1383–1392. [[CrossRef](#)]
32. Hu, T.T.; Yoshie, R. Indices to evaluate ventilation efficiency in newly-built urban area at pedestrian level. *J. Wind Eng. Ind. Aerod.* **2013**, *112*, 39–51. [[CrossRef](#)]



© 2019 by the authors. Licensee MDPI, Basel, Switzerland. This article is an open access article distributed under the terms and conditions of the Creative Commons Attribution (CC BY) license (<http://creativecommons.org/licenses/by/4.0/>).